Tuning the Interfacial Electronic Structure of MoS$_2$ by Adsorption of Cobalt Phthalocyanine Derivatives

Philipp Haizmann[1], Eric Juriatti[1], Maren Klein[1], Katharina Greulich[1], Ruslan Ovsyannikov[3], Erika Giangrisostomi[3], Thomas Chassé[1], Heiko Peisert[1,*], Marcus Scheele[1,2,*]

1 Institut für Theoretische und Physikalische Chemie, Universität Tübingen, 72076 Tübingen, Germany

2 Center for Light-Matter Interaction, Sensors & Analytics LISA+, Universität Tübingen, 72076 Tübingen, Germany

3 Institute Methods and Instrumentation for Synchrotron Radiation Research, Helmholtz-Zentrum Berlin für Materialien und Energie GmbH, 12489 Berlin, Germany

*To whom correspondence should be addressed:

Heiko.Peisert@uni-tuebingen.de and Marcus.Scheele@uni-tuebingen.de

Keywords

Transition Metal Dichalocogenides, Angle Resolved Photoelectron Spectroscopy (ARPES), XPS, UPS, Doping, Induced Gap State, Heterostructure

1

ABSTRACT

We investigate the interfacial electronic structure of n-type bulk MoS_2 upon the adsorption of CoPc and $CoPcF_{16}$ mono- and few-layers using advanced spectroscopic techniques. These include X-ray photoelectron spectroscopy (XPS), X-ray absorption spectroscopy (XAS), angle-resolved photoelectron spectroscopy (ARPES), and ultraviolet photoelectron spectroscopy (UPS). Our findings indicate that the adsorption of CoPc enhances the degree of n-doping at the interface with MoS_2. In contrast, $CoPcF_{16}$ results in a nearly intrinsic position of the Fermi level. Furthermore, we note the formation of an induced gap state near the valence band maximum for monolayer $CoPcF_{16}$ on MoS_2. These observations underscore the potential to fine-tune the interfacial electronic properties of transition metal dichalcogenides through molecular functionalization for tailored electronic applications.

INTRODUCTION

As electronic component miniaturization progresses, innovative materials and their unique interactions become pivotal to the ongoing evolution of semiconductor devices. Transition metal dichalcogenides (TMDCs), such as molybdenum disulfide (MoS_2), have gained significant attention in this context. These materials possess a layered crystal structure, tunable bandgaps and high carrier mobilities, making them especially appealing for use in optoelectronics, photovoltaics and field-effect transistors.[1-5] To further refine these semiconductor components for targeted applications, merging TMDCs with organic semiconductors is a promising strategy, also because it preserves the structural integrity of the TMDCs.[6] Past endeavors in this direction have involved functionalization with strong electron acceptors such as (fluorinated) tetracyanoquinodimethane (TCNQ)[7-11], fluorinated fullerenes[12], and 4-nitrobenzenediazonium tetrafluoroborate (4-NBD)[13], all of which induce p-type doping of the TMDC by integer charge transfer. Similarly, n-doping has been achieved through

2

functionalization with different organic and inorganic heterostructures.[11, 13-19] A large portion of research was dedicated to mono- and few-layer TMDCs and there are few studies that deal with bulk crystals and even less with heterostructures. Given that the number of layers is crucial for the properties of the electronic structure, expanding the research to bulk crystals is necessary to gain a deeper understanding of heterostructures from organic molecules and TMDCs.

Transition metal phthalocyanines (TPcs) are a versatile class of organic semiconductors. Their inherent chemical variability makes them especially intriguing for studies focused on organic-inorganic semiconductor heterostructures. A key aspect of TPcs is the substitutability of the central atom and the alterability of peripheral positions, like fluorination, which significantly impacts their ionization energy and affects energy level alignments in heterostructures (e.g. Ref.[20-22]) Notably, phthalocyanines are anticipated to exhibit weak interactions on van der Waals surfaces. Such interactions can be beneficial for customizing the electronic properties of TMDCs, since a strong interaction, accompanied by an integer charge transfer, would result in an undesirable localization of the charges at the interface.

By constructing such weakly interacting TMDC/TPc heterostructures, the photoresponsivity and response time in phototransistors were improved compared to the pure TMDC components.[23-27] Furthermore, TPcs could be used for defect engineering and the resulting enhancement of photoluminescence quantum yields.[28-30] In this work, we seek to modify the type and concentration of charge carriers in n-type MoS_2 by adsorption of cobalt-phthalocyanine (CoPc) and its perfluorinated derivative ($CoPcF_{16}$). While the interface between TMDCs and other TPcs has been explored previously, the effect of the cobalt derivatives has not been studied so far.[31] Moreover, this work contributes to the understanding of charge transfer processes and interface states in general which is still under investigation.[32-35]

Using synchrotron-based X-ray photoelectron spectroscopy (XPS), X-ray absorption spectroscopy (XAS), and angle-resolved photoemission spectroscopy (ArPES), complemented

3

by ultra-violet photoelectron spectroscopy (UPS) and a laboratory-source XPS, we systematically examine the interface of these heterostructures. Our results indicate that it is possible to tune the properties of MoS_2 merely by the choice of CoPc $vs.$ $CoPcF_{16}$. We find evidence for the formation of an induced gap state with $CoPcF_{16}$, which is absent with CoPc. This research provides important insights into tuning the semiconductor properties of TMDC-based devices.

EXPERIMENTAL

All experiments were conducted either at the LowDosePES endstation of the PM4 beamline (BESSY II, Helmholtz-Zentrum Berlin, Germany)[36, 37] or with our laboratory setup under ultra-high vacuum (UHV) conditions (base pressure at the LowDosePES endstation $1 \cdot 10^{-10}$ mbar and $5 \cdot 10^{-10}$ mbar at our home system). At the LowDosePES, the clean MoS_2 surface was examined with XAS, XPS and ArPES using an angle-resolved time-of-flight detector (ARTOF).[37] This detector offers high efficiency compared to conventional hemispherical analyzers, thus enabling experiments at lower photon flux, mitigating potential radiation damage to phthalocyanines in prolonged experiments with longer radiation exposure times. XAS measurements were carried out in the total electron yield mode measuring the sample current. For energy calibration we used a gold single crystal which was cleaned by repeated cycles of argon ion sputtering and annealing. After each change of the excitation energy, the **Au***4f*$_{7/2}$ (84.00 eV) binding energy was measured, and consecutive measurements calibrated to this. For photoemission experiments with excitation energies of 900, 300, 230 and 75 eV an energy resolution of 1492, 188, 133 and 69 meV was estimated, respectively. For the ArPES measurements, we utilized a photon energy of 75 eV and chose a detector acceptance angle of 30 degrees to probe with a maximum $k_\parallel$ value of approximately 1.16 Å^{-1}. We chose this photon energy as for a good compromise between intensity and reciprocal space resolution and extension. The calculated distances in the reciprocal space from Γ to K is 1.325 Å^{-1} and 1.147

4

Å^{-1} from Γ to M for the hexagonal MoS$_2$ lattice with a lattice constant of 3.162 Å.[38] It was possible to probe the full Brillouin zone at this energy, provided the sample is titled such that the gamma point ends up at the edge of the detector field of view (see **Figure S1**, Supporting Information). Using the k_x versus k_y momentum map, we traced the path through reciprocal space from K to Γ to M and plot the energy dispersion diagrams (see red lines in **Figures 2e** and **f**).

At the home-based spectrometer, a monochromatized aluminum Kα source (XR 50 M, Specs) and a duoplasmatron type discharge UV light source (UVS 300, Specs) were employed for XPS and UPS measurements, respectively. Energy calibration at the home-based spectrometer was performed using Au, Ag and Cu foils (Goodfellow Cambridge Ltd.), which were also cleaned by argon ion sputtering, calibrating to the binding energies of **Au**$4f_{7/2}$ (84.00 eV), **Ag**$3d_{5/2}$ (368.21 eV) and **Cu**$2p_{3/2}$ (932.63 eV). Here, the energy resolution for XPS and UPS were 400 meV and 150 meV, respectively. Molybdenum disulfide (2H-MoS$_2$) crystals were purchased from 2D Semiconductors Inc. and fixed to sample holders with silver glue. To ensure a clean surface the MoS$_2$ crystals were cleaved *in situ* using adhesive tape. Successful cleavage was evidenced by a carbon- and oxygen-free surface, as confirmed by XPS and work function measurements (home lab). Phthalocyanines (Porphyrin Systems Hombrecher e.K. and Sigma Aldrich) were deposited on the prepared surfaces under UHV conditions using molecular beam epitaxy. A Knudsen cell and resistive heating in the range of 390 - 410 °C were employed for deposition. The deposition rate was monitored with a quartz crystal microbalance and the temperature adjusted to reach an approximate rate of 0.2 nm/min. The nominal layer thickness was determined by photoemission, comparing the intensities of the **C**$1s$ and **Mo**$3d$ core levels (**Figure S2**, Supporting Information). Photoionization cross sections were taken from Yeh and Lindau[39] and employed for calculations, while the inelastic mean free path of photoelectrons was determined according to Seah and Dench.[40] For each series of experiments, a crystal was

5

freshly cleaved. Different crystals were used for the experiments, but care was taken to ensure that specific phthalocyanines were only studied with certain crystals, preventing any cross-contamination.

RESULTS AND DISCUSSION

The energy level alignment and position of the Fermi level can be, in a first approximation, indirectly monitored via the binding energy of the substrate core level peaks, assuming rigid shifts of core and valence band levels (e.g. Ref. 41). **S**$2p$ and **Mo**$3d$ core level spectra, (measured at the LowDosePES endstation and at our home setup) are presented in **Figure 1**. We choose low excitation energies for the synchrotron experiments to ensure that the measurements are as surface-sensitive as possible. For details on the calculation of the inelastic mean free paths for all experiments and photon energies we refer to the Supporting Information (**Table S1**). Briefly, the experiments at the LowDosePES endstation probe mostly the first layer, considering an MoS_2 monolayer thickness of about 0.7 nm.[42] In contrast, the experiments at the lab spectrometer with an Al Kα source and an inelastic mean free path of the photoelectrons of about 2.4 nm are more volume-sensitive. **Figures 1a** and **b** display the **S**$2p$ core-level spectra, collected at an excitation energy of 230 eV before and after the exposure of MoS_2 to CoPc and CoPcF$_{16}$, respectively. Similarly, **Figure 1c** and **d** depict the **Mo**$3d_{5/2}$ core-level spectra, recorded at an excitation energy of 300 eV for the same two interfaces. The layer thicknesses of 0.34 nm corresponds approximately to a monolayer coverage,[43] whereas thicker films of 1.16 nm (CoPc) and 1.71 nm (CoPcF$_{16}$) represent multilayers in the case of flat lying molecules. The spectra of the freshly cleaved surfaces which serve as reference points, are represented in black in both figures. The binding energies of the **Mo**$3d_{5/2}$ signals (229.20 eV (**Figure 1a**) and 229.25 eV (**Figure 1b**)) and **S**$2p_{3/2}$ (162.15 eV (**Figure 1c**) and 162.20 eV (**Figure 1d**)) are typical for 2H-MoS$_2$.[44, 45] Although we observe a slight difference of 50 meV between the fresh samples (e.g. due to different defect densities)[46, 47], we do not expect a great influence from this

6

difference on the interaction between the MoS_2 and the phthalocyanines. The deposition of the first layer of CoPc and $CoPcF_{16}$ causes a binding energy shift of the MoS_2 core-level spectra. A shift of 0.3 eV towards higher binding energies (**Mo***$3d_{5/2}$* at 229.50 eV and **S***$2p_{3/2}$* at 162.45 eV) is observed after the deposition of the first CoPc layer (illustrated by the light green curves in the figures). Conversely, with $CoPcF_{16}$ there is a decrease of 0.3 eV (**Mo***$3d_{5/2}$* at 228.93 eV and **S***$2p_{3/2}$* at 161.90 eV) in binding energy (represented by the light lilac curves in the figures). The deposition of subsequent layers of the phthalocyanines has a comparably negligible effect (curves in darker shades of green and lilac). In the more volume-sensitive experiments on the laboratory spectrometer, we obtain the same result for the CoPc/MoS_2 heterostructure (**Figures 1e** and **f**). In contrast, with $CoPcF_{16}$ (**Figures 1g** and **h**) no shift to lower binding energy is observed. This indicates that the interaction primarily occurs on the top layer of the molybdenum disulfide.

7
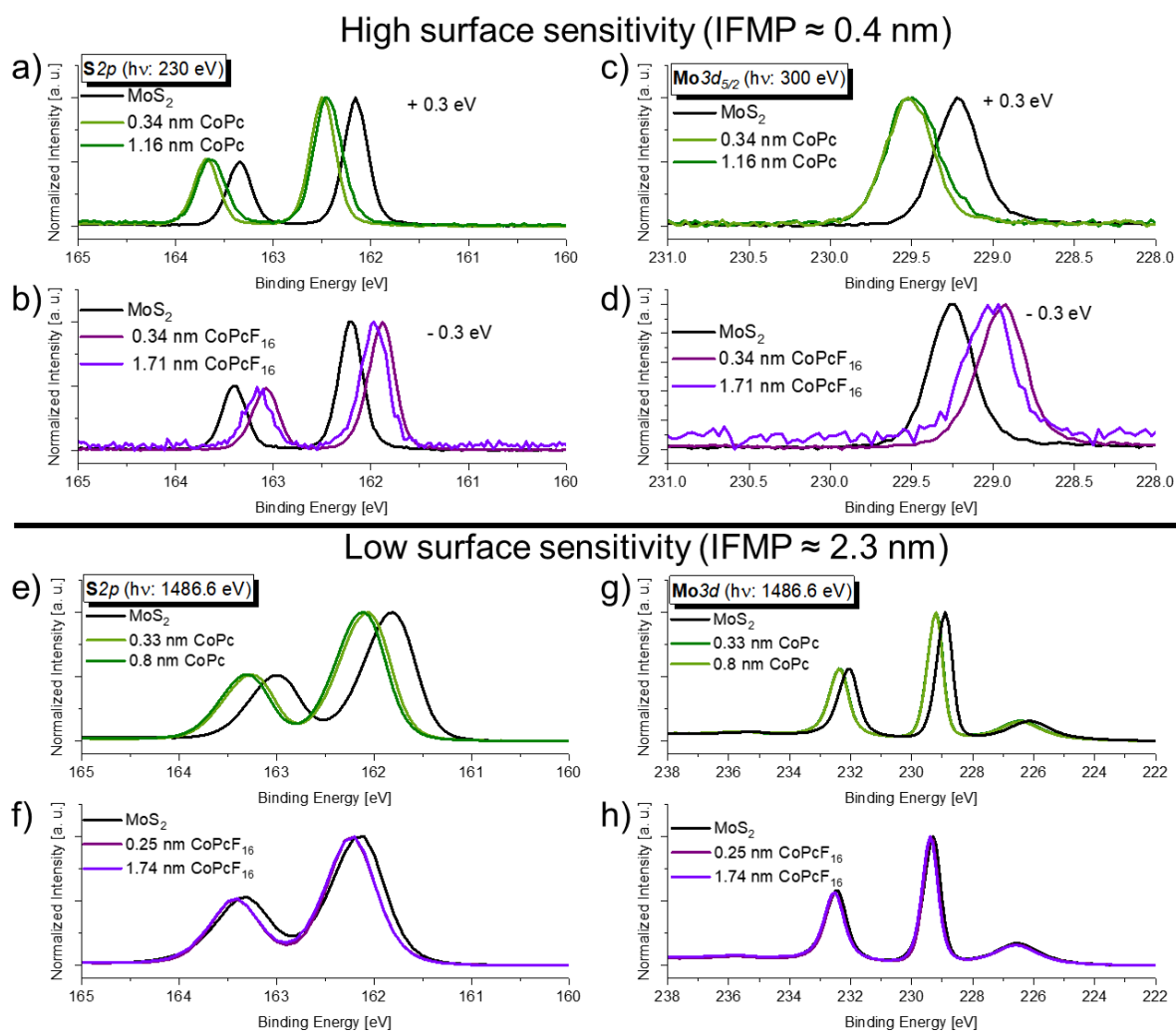
Figure 1 X-ray Photoelectron Spectroscopy (XPS) measurements of the core-levels of MoS_2 following deposition of CoPc and $CoPcF_{16}$. The spectra of the freshly cleaved surfaces appear in black. Green and lilac colors correspond to shifts in binding energy following the deposition of the CoPc and $CoPcF_{16}$ layers respectively. **S**$2p$ core-level spectra for MoS_2 with CoPc shown in (**a**) and (**e**) and with $CoPcF_{16}$ shown in (**b**) and (**f**). **Mo**$3d$ core-level spectra for MoS_2 with CoPc shown in (**c**) and (**g**) and with $CoPcF_{16}$ shown in (**d**) and (**h**). Spectra in (**a**), (**b**), (**c**) and (**d**) acquired at LowDosePES end-station, spectra in (**e**), (**f**), (**g**) and (**h**) acquired at the home setup.

Generally, shifts of core level binding energies of semiconductor materials (as probed by XPS) can be caused either by changes in the (chemical) environment of the considered atom,

8

or by the variation of the position of the reference level, the Fermi level. In the present case, the quantitatively identical shift of the positions of the **Mo***3d* and the **S***2p* binding energies, indicate a shift of the substrate Fermi level because of the deposition of molecules, that is, an (interface) doping. Such doping-related core level shifts are well-known: For example, for silicon the **Si***2p* binding energy of heavily n-doped silicon is found at higher values compared to heavily p-doped silicon.[48] These findings fit well to other previous investigations of doping in different heterostructured TMDCs.[12, 13, 19, 49]

To gain a deeper understanding of the origin of this doping, we map the band structure obtained by angle-resolved photoelectron spectroscopy (ARPES) in **Figure 2. Figures 2a** and **b** display the energy dispersion diagrams for freshly cleaved MoS$_2$, while **Figures 2c** and **d** depict the diagrams after deposition of monolayers (0.34 nm) of CoPc and CoPcF$_{16}$, respectively. All energy dispersion diagrams were extracted from cuts through the momentum maps shown in **Figures 2e** and **f** and the paths are indicated by the red lines. We omit the dispersion diagrams for the thicker films here, as the method is highly surface-sensitive, and substrate-related features are no longer visible, which makes tracing a comparable momentum cut not reliable. To further illustrate changes upon deposition, **Figures 2g** and **h** represent the integration over the imaged area of the detector for all spectra. The intensity is normalized to facilitate a comparison. The valence band maxima (VBM) at the Γ point for the two freshly cleaved substrates were found at 0.92 and 0.77 eV (**Figures 2a** and **b**), indicating slight n-type doping, when considering a band gap of 1.23 eV.[50] We note that even in-situ cleaved samples can exhibit a slightly different position of the Fermi level, depending crucially on the number of step edges and other defects in the analyzed area. However, the careful monitoring of the measurement spot (diameter 0.1 mm) on the sample enables the analysis of the same sample region before and after the deposition of the molecules. For CoPc deposition, we observe a positive shift (+ 0.21 eV) of the Γ point to 1.13 eV, while for CoPcF$_{16}$ deposition, the Γ point

9

moves (- 0.11 eV) to 0.66 eV. The direction of these shifts is consistent with the results obtained from XPS core-level measurements, but it is worth noting that the magnitude of these shifts is different. This shows that rigid shifts in the measured core-level provide a qualitative indication of changes in the Fermi level's position. However, for a more precise analysis, the valence band region must be examined.

The same ARPES measurements also reveal details about the electronic properties of the deposited molecular monolayers. For CoPc (**Figure 2c**), we locate the HOMO (Highest Occupied Molecular Orbital) maximum at around 0.9 eV and the on-set at around 0.6 eV, e.g. slightly above the energy of the VBM of MoS_2. As expected for phthalocyanines, we find an intensity variation depending on the angle of emitted electrons with the highest state density around 1.5 - 1.7 Å^{-1}, [51-53] that is, in the vicinity of the K- and M-point of MoS_2 visible in the momentum maps at 0.8 eV shown in **Figure 2e**. We note that for thicker CoPc films, the HOMO maximum is found at 1.05 eV (**Figure 2g**) and the on-set at around 0.75 eV. A possible reason might be that screening effects at the interface occur in both the MoS_2 and the CoPc, which has also been observed for phthalocyanines on metal substrates.[54, 55] When fitting the HOMO peaks of the monolayer and thicker CoPc films with an Gaussian function we find two different full width half maxima (FWHM) of 0.36 and 0.4 eV respectively. Those differences can be explained by an inhomogeneous film growth but also by molecule-molecule interactions,[56, 57] which also cause energetic shifts of the HOMO.
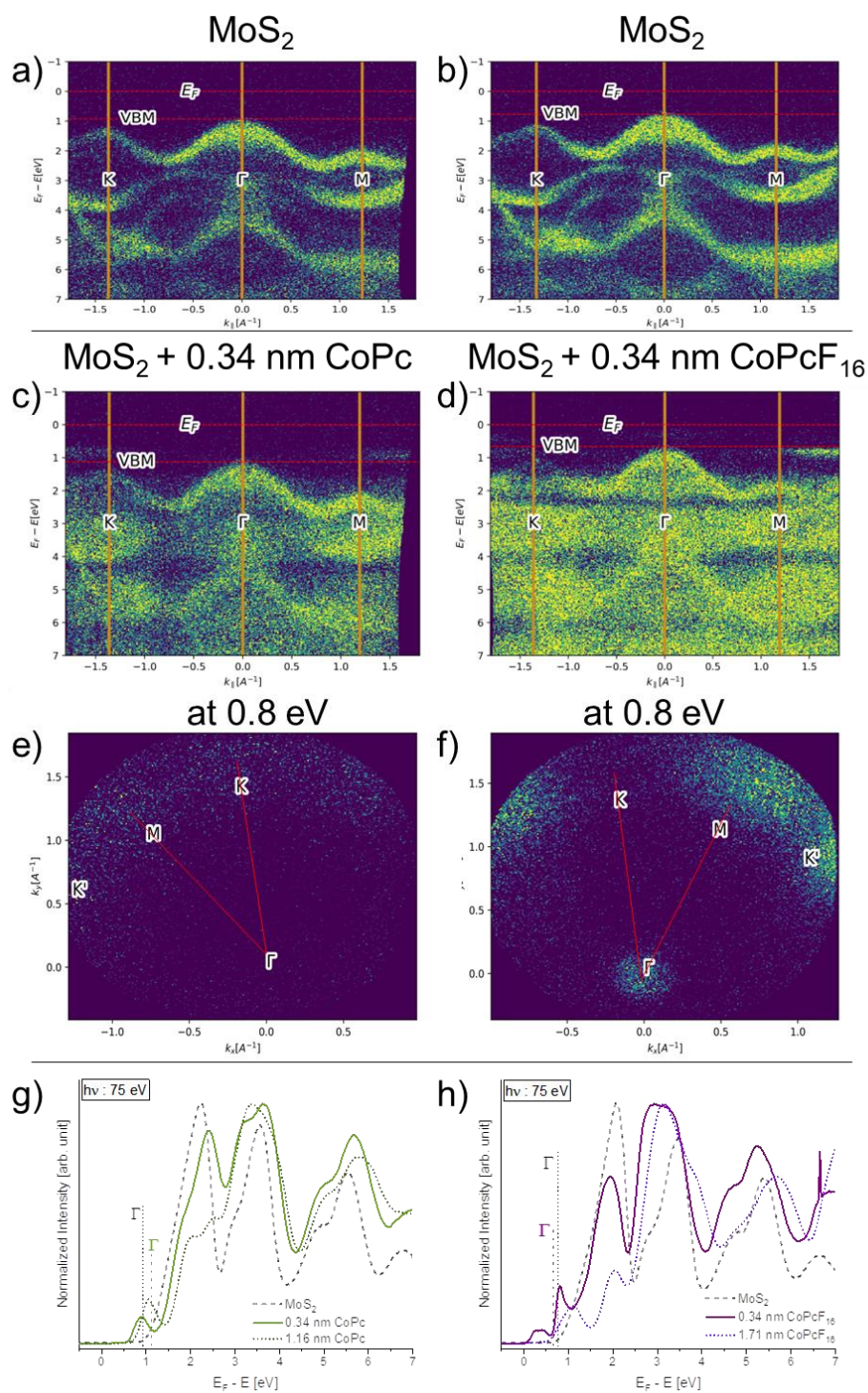
Figure 2 (**a – d**) Energy dispersion diagrams for different pathways through the Brillion zone. (**a**) and (**b**) show measurements of the clean surface while (**c**) and (**d**) show the dispersion diagrams after deposition of CoPc and CoPcF$_{16}$ respectively. In (**e**) and (**f**), momentum maps at 0.8 eV are show for the respective CoPc/MoS$_2$ and CoPcF$_{16}$/MoS$_2$ heterostructures. The red

11

lines indicate the cuts taken to obtain the energy dispersion diagrams for (**a – d**). In (**g**) and (**h**) the integrated and normalized spectra for the clean MoS_2 crystals and after deposition of the respective phthalocyanines are shown.

For $CoPcF_{16}$ (**Figure 2d**), we locate the HOMO maximum at around 0.8 eV with the highest state density again near the K- and M-points (see momentum map in **Figure 2f**), an on-set at 0.65 eV (**Figure 2h**) and a FWHM of 0.3 eV. Different from CoPc, an additional, more diffuse state emerges near the Γ point with its maximum at 0.35 eV and an on-set close to the Fermi level at 0.1 eV (see also **Figure 2h** and **Figure S1c**, Supporting Information). For thicker molecular films, this state disappears, the HOMO maximum shifts to 1.11 eV with an on-set at 0.6 eV, and the FWHM broadens to 0.55 eV. Thus, the effects displayed in **Figure 2** are confined to the interface.

We discuss the most likely provenance of this new state in the context of three established mechanisms of charge transfer (CT), namely integer charge transfer (ICT)[58-61], fractional charge transfer (FCT)[62-64], and induced gap states (IGS)[65-67]. All concepts can be used to describe CT processes at organic/inorganic interfaces of semiconductor heterostructures, and for details we refer to the Supporting Information.

Based on our observation that the interaction in the $CoPcF_{16}/MoS_2$ system is limited to the first MoS_2 layer, while in the $CoPc/MoS_2$ system the interaction is more extensive, we propose that the interaction is best described by the IGS model. We will later present this in an energy level alignment (ELA) diagram summarizing all measurement results. However, it is worth noting now that the interaction in $CoPc/MoS_2$ can be explained through the formation of a macroscopic dipole, whereas the $CoPcF_{16}/MoS_2$ system needs to be described within the IGS framework, involving the formation of microscopic dipoles at the interface.

For completeness, we aim to consider the entire system and subsequently discuss our results in relation to other models. Therefore, one alternative explanation for the new state near the

12

Fermi level could also be the occupation of the CoPcF$_{16}$ LUMO at the interface with MoS$_2$, similar to previous studies of diamond and F4-TCNQ, its anionic derivative,[58, 68] as well as for pentacene on copper.[69] This would be in the framework of the ICT model and could explain the observed core level shift of MoS$_2$ due to p-doping and a localized charge transfer, accommodated with a reduction of negative charge carriers in the MoS$_2$. However, for such a scenario one would expect a LUMO-like distribution in the momentum maps, that is, with zero density at the Γ-point.[53] A close examination of the momentum map at 0.35 eV (**Figure S1c**, Supporting Information) shows significant density at the Γ-point, which therefore excludes a charge transfer into the CoPcF$_{16}$ LUMO.

The formation of a gap state in the substrate for CoPcF$_{16}$/MoS$_2$ can cause local interfacial charge transfer and also hybridization in the context of FCT. To study if the central atom (Co) of the phthalocyanines is involved in such an interaction, we perform X-ray absorption (XAS) experiments at the Co-L$_3$ edge and XPS measurements of the **Co$2p_{5/2}$** region, presented in **Figure 3**. Metal L-edge spectra of TMPcs are in particular sensitive to changes of the configuration of d-electrons.[70] In the case of an occupation or hybridisation of particular orbitals, excitation cannels can be blocked, as shown for CoPc on Ni and grapene/Ni.[71]

The XAS results for mono- and multilayer deposition of CoPc are displayed in **Figure 3a**, while the corresponding results for CoPcF$_{16}$ are shown in **Figure 3b**. Most notably, there are no significant differences in the spectra for each molecule obtained after monolayer vs. multilayer deposition. This indicates that the observed induced gap state in **Figure 2** is not localized on the Co atom, as the peak shape and position would be expected to change otherwise.
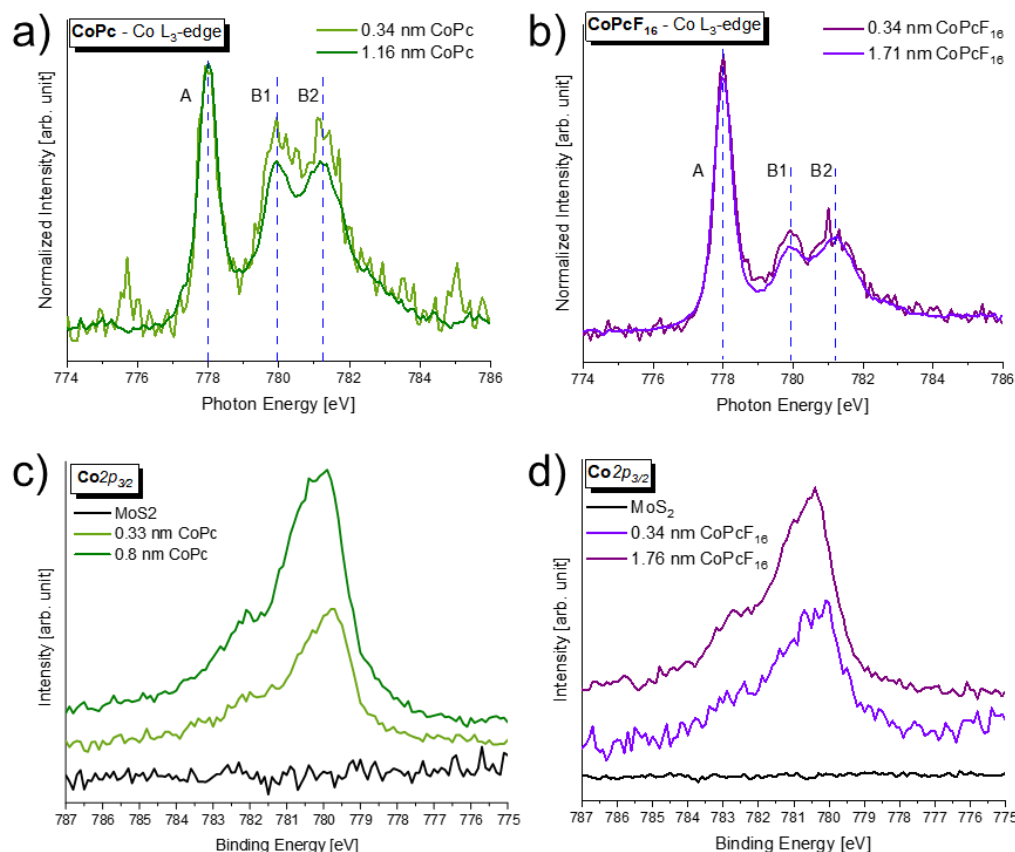
Figure 3 (**a**) and (**b**) show XAS measurements (acquired at LowDosePES) on the Co L$_3$-edge region after depositon of CoPc and CoPcF$_{16}$ respectively. In (**c**) and (**d**) XPS measurements (acquired at the home lab) of the **Co$2p_{3/2}$** region are shown for similar thicknesses of CoPc and CoPcF$_{16}$ respectively.

XPS experiments of the **Co$2p_{3/2}$** region after CoPc or CoPcF$_{16}$ deposition (**Figure 3e and f,** repectively) support our hypothesis that the Co atom does not take part in charge transfer since there are no variations in the spectral shapes after monolayer vs. multilayer deposition.

To test whether the interaction involves the organic macrocycle, we analyzed the **C$1s$** region in more detail after CoPc or CoPcF$_{16}$ deposition (**Figure 4a and b,** respectively, with fitting parameters and peak positions listed in **Table S1,** and a detailed description of the fitting procedure in the Supporting Information).[4, 72] Three chemically distinct carbons can be identified marked in the chemical structure shown in **Figure 4**. Those are the ones bound to

14

nitrogen (C1), the neighboring carbon (C2) and the peripheral carbons bound either to hydrogen or fluorine atoms depending on the moiety under consideration (C3). We note a slight shift to higher binding energies of the CN components for multilayers vs. monolayers, indicating screening effects at the interface and/or a possible site-dependent redistribution of electrons.[54,72] This might be a hint for a redistribution of electrons at the interface due to local interactions, but differences between the phthalocyanine monolayer in direct contact with the MoS_2 surface and the thick film are minor. Similar results were obtained for the laboratory-source measurements, although the lower energy resolution causes a broadening of the Gaussian width (see **Figure S1** and **Table S2**, Supporting Information). On this basis, we can rule out hybridization in the context of an FCT. At the same time, these investigations suggest that the macrocycle has a small contribution to the formation of the IGS, and this is limited to the interface, specifically the first TPc monolayer.

15
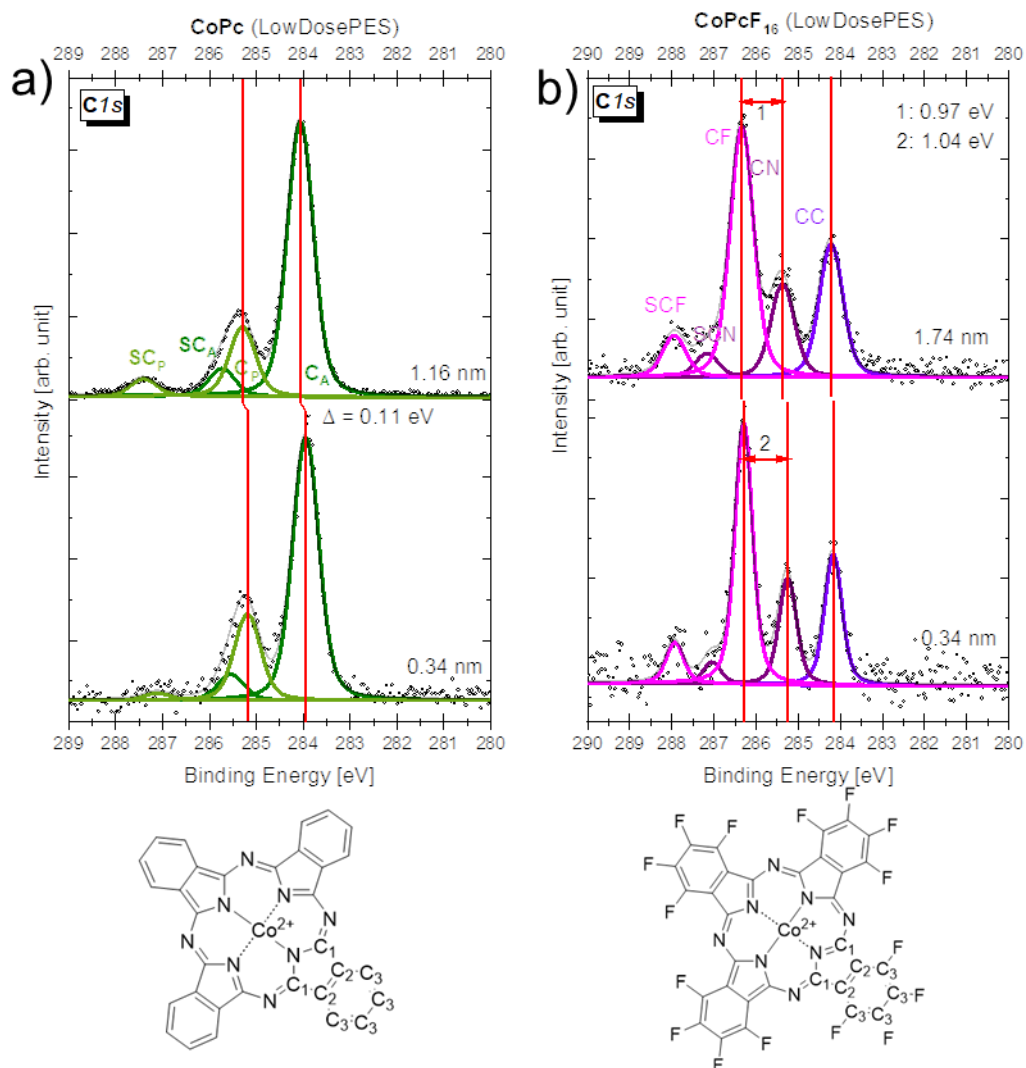
Figure 4 C1s core-level spectra of the phthalocyanine ML and thick film. (**a**) shows the measured data and applied fit model for CoPc (upper part for the 1.16 nm film and lower part for the phthalocyanine monolayer). Below the spectra, the chemically inequivalent carbon atoms are marked as C1 - C3. In (**b**) the results for the perfluorinated CoPcF16 is displayed.

We combine all electronic structure information derived so far to construct the energy level alignment (ELA) diagrams in **Figure 5**. Further, we include results from the work function and UV-Vis absorption measurements shown in **Figure S4**, Supporting Information. The work functions are extracted from the determination of the secondary electron cutoff in the UPS experiments. For freshly cleaved surfaces of MoS_2, we find a work function of 5.1 eV. After deposition of roughly a monolayer CoPc, the work function decreases to 4.8 eV. Depositing an

16

even thicker film, the work function continues to decrease to 4.5 eV. In contrast, for $CoPcF_{16}$ deposition the work function increases to 5.3 eV after one monolayer, and no further changes occur for thicker films. These findings suggest that CoPc induces a strong negative dipole change of $-$ 0.6 eV at the MoS_2 surface. This change of the surface dipole and the accommodated band-banding observed in the core-level shifts is consistent with our previous results with iron-phthalocyanines[22] as well as for other heterostructures of MoS_2, for example with cesium carbonate.[16] In contrast, $CoPcF_{16}$ induces a weak positive dipole change of $+$ 0.2 eV. The optical bandgaps are 1.66 eV and 1.54 eV, consistent with values for similar phthalocyanines (**Figures S2c** and **d** respectivly).[20, 74, 75] We assume that pure phthalocyanines behave identically to thick multilayers deposited on MoS_2 and compare the electronic structure of pure CoPc as well as $CoPcF_{16}$ with freshly cleaved MoS_2 in **Figures 5a** and **5c**, respectively. For the ELA construction, we neglect energy dispersions and band structure information and just evaluate the VBM (energy at the Γ point) and the CBM (based on optical band-gap measurements taken from literature).[50] The same representation is done with the phthalocyanines as we take the HOMO on-sets and the measured optical band-gap to place the LUMO accordingly. From this, we infer a staggered gap of the frontier orbitals of CoPc with the band edges of MoS_2 before contact, i.e. for vacuum level alignment. For $CoPcF_{16}$ however, we suggest that the VBM and the HOMO are roughly at the same energy before contact.
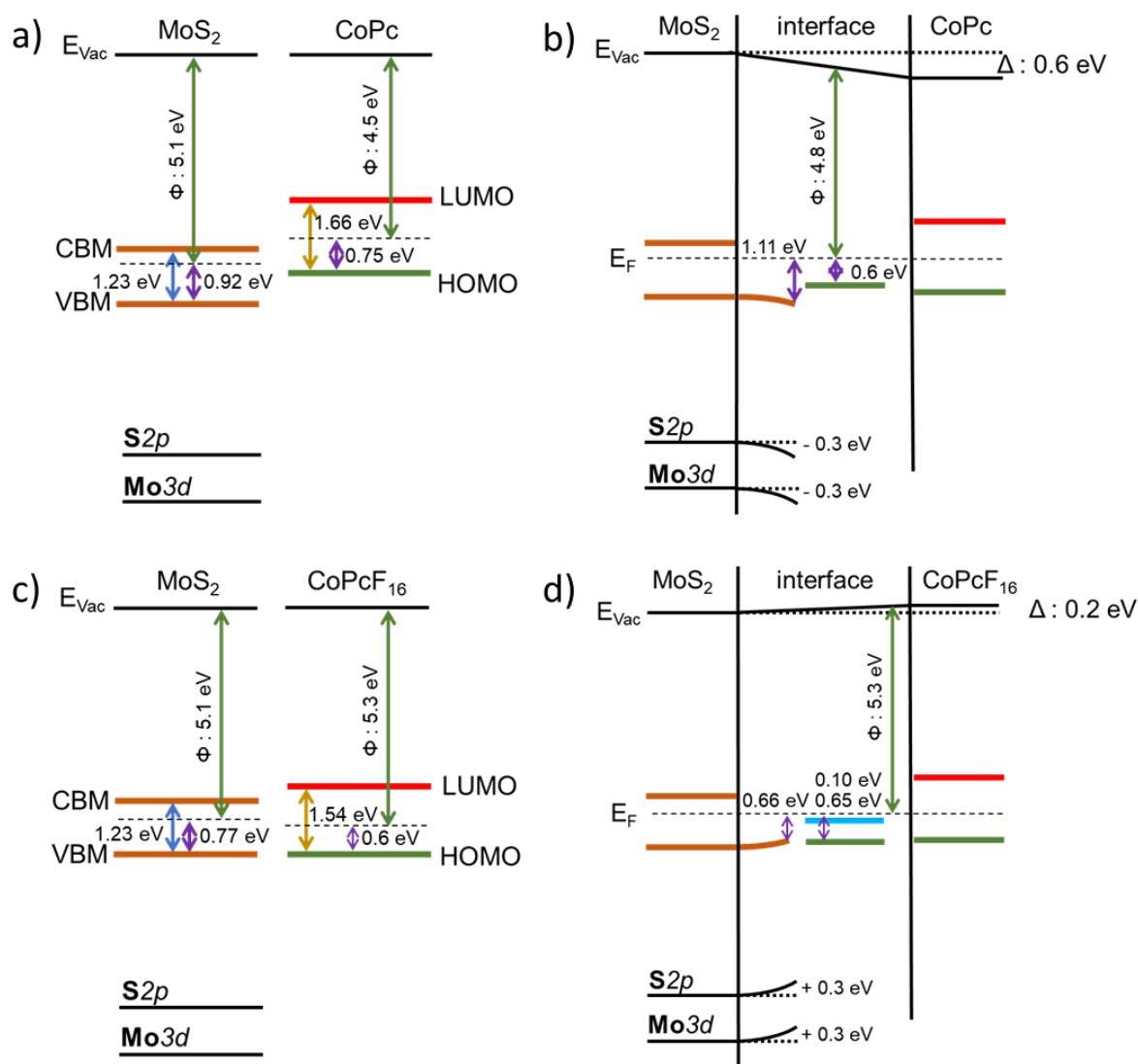
Figure 5 Energy level alignment diagrams. All arrows represent measured data, except for the band-gap of MoS₂ which is taken from literature[50]. Green arrows are obtained from UPS measurements at the lab spectrometer (**Figures S4a** and **b**). Values for the purple arrows are taken from the integrated ARPES measurements (**Figures 2g** and **h**). Yellow arrows represent the values taken from UV-Vis absorption measurements of the respective phthalocyanine films on glas substrates (**Figures S4a** and **b**). (**a**) and (**c**) show MoS₂ and CoPc/CoPcF₁₆ before contact, respectively. The energy levels of the MoS₂ VBM (Γ-point) are represented as single values and the position of the CBM placed based on a band gap value of 1.23 eV.[50] For the HOMOs of the phthalocyanines, the measured onset values are shown in green. Since no information besides the optical band gap is measured for the LUMO of the phthalocyanines, a

18

single energy level is shown (red). The alignment for (**a**) and (**c**) is on the vacuum niveau. (**b**) and (**d**) show MoS_2 and CoPc or $CoPcF_{16}$ in contact, i.e. with Fermi-levels aligned.

From **Figure 5c**, no integer charge transfer from MoS_2 to $CoPcF_{16}$ is expected since the LUMO of $CoPcF_{16}$ is located above the CB of MoS_2, and compared to other electron acceptors the electron affinity is significantly lower. Nevertheless, we find p-type doping of the MoS_2. We can deduct that only a new induced gap state at the MoS_2/$CoPcF_{16}$ interface can explain the charge transfer, best described on the basis of the IGS model. We note that the formation of induced gap states at interfaces is known for several organic-metal interfaces and for organic-inorganic semiconductor interfaces.[32, 66, 76, 77]

CONCLUSION

We presented a comprehensive XPS/ARPES and XAS study on the heterostructure system of CoPc and $CoPcF_{16}$. Our findings show that CoPc and $CoPcF_{16}$ can both be used for Fermi level engineering of bulk MoS_2, however with notable differences in the mechanism of their action. CoPc induces a surface dipole and a downwards band bending, which is consistent with previous findings for other phthalocyanines. The influence of adsorbed CoPc extends into multiple layers of the MoS_2 substrate. In contrast, the n-type character of MoS_2 is reduced through interaction with $CoPcF_{16}$. The results of the study suggest the presence of an induced gap state, and the interaction is limited to only the first layer of the MoS_2 bulk crystal. While this study has focused on the interface of bulk MoS_2, the question remains open as to whether these findings can be directly transferred to heterostructures with two-dimensional MoS_2. The electronic structure of two-dimensional MoS_2 differs from that of bulk crystals. However, the effects described here are found directly at the interface, which could make them highly relevant for these materials as well.

ACKNOWLEDGEMENTS

19

SUPPORTING INFORMATION

In this section, we present additional momentum maps recorded at the LowDosePES endstation. We also discuss overview spectra used for quantifying layer thicknesses. Besides C1s spectra measured in the home laboratory, a detailed description of C1s fit models and the parameters used are provided. Conclusively, measurements of work functions and UV-Vis absorption are presented, along with a brief explanation of interface models related to charge transfer (CT).

GRAPHICAL ABSTRACT
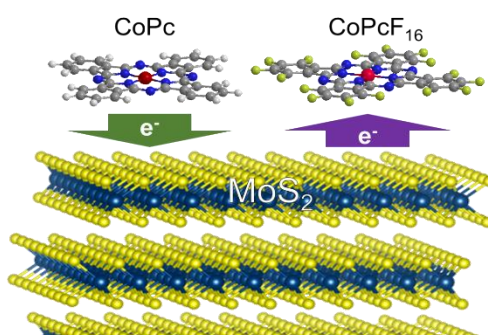
REFERENCES

(1) Jariwala, D.; Sangwan, V. K.; Lauhon, L. J.; Marks, T. J.; Hersam, M. C. Emerging device applications for semiconducting two-dimensional transition metal dichalcogenides. *ACS Nano* **2014**, *8* (2), 1102-1120, DOI: 10.1021/nn500064s.

(2) Wang, Q. H.; Kalantar-Zadeh, K.; Kis, A.; Coleman, J. N.; Strano, M. S. Electronics and optoelectronics of two-dimensional transition metal dichalcogenides. *Nat Nanotechnol* **2012**, *7* (11), 699-712, DOI: 10.1038/nnano.2012.193.

(3) Wang, H.; Li, C.; Fang, P.; Zhang, Z.; Zhang, J. Z. Synthesis, properties, and optoelectronic applications of two-dimensional MoS(2) and MoS(2)-based heterostructures. *Chem Soc Rev* **2018**, *47* (16), 6101-6127, DOI: 10.1039/c8cs00314a.

(4) Schmidt, H.; Giustiniano, F.; Eda, G. Electronic transport properties of transition metal dichalcogenide field-effect devices: surface and interface effects. *Chem Soc Rev* **2015**, *44* (21), 7715-7736, DOI: 10.1039/c5cs00275c.

(5) Radisavljevic, B.; Radenovic, A.; Brivio, J.; Giacometti, V.; Kis, A. Single-layer MoS2 transistors. *Nat Nanotechnol* **2011**, *6* (3), 147-150, DOI: 10.1038/nnano.2010.279.

(6) Huang, Y. L.; Zheng, Y. J.; Song, Z.; Chi, D.; Wee, A. T. S.; Quek, S. Y. The organic-2D transition metal dichalcogenide heterointerface. *Chem Soc Rev* **2018**, *47* (9), 3241-3264, DOI: 10.1039/c8cs00159f.

(7) Nevola, D.; Hoffman, B. C.; Bataller, A.; Ade, H.; Gundogdu, K.; Dougherty, D. B. Rigid valence band shift due to molecular surface counter-doping of MoS2. *Surface Science* **2019**, *679*, 254-258, DOI: 10.1016/j.susc.2018.09.016.

(8) Park, S.; Schultz, T.; Xu, X.; Wegner, B.; Aljarb, A.; Han, A.; Li, L.-J.; Tung, V. C.; Amsalem, P.; Koch, N. Demonstration of the key substrate-dependent charge transfer mechanisms between monolayer MoS2 and molecular dopants. *Commun. Phys.* **2019**, *2* (1), 109, DOI: 10.1038/s42005-019-0212-y.

(9) Jing, Y.; Tan, X.; Zhou, Z.; Shen, P. Tuning electronic and optical properties of MoS2monolayer via molecular charge transfer. *J. Mater. Chem. A* **2014**, *2* (40), 16892-16897, DOI: 10.1039/c4ta03660c.

(10) Wang, J.; Ji, Z.; Yang, G.; Chuai, X.; Liu, F.; Zhou, Z.; Lu, C.; Wei, W.; Shi, X.; Niu, J.; et al. Charge Transfer within the F4TCNQ-MoS2 van der Waals Interface: Toward Electrical Properties Tuning and Gas Sensing Application. *Adv. Funct. Mater.* **2018**, *28* (51), 1806244, DOI: 10.1002/adfm.201806244.

(11) Mouri, S.; Miyauchi, Y.; Matsuda, K. Tunable photoluminescence of monolayer MoS(2) via chemical doping. *Nano Lett* **2013**, *13* (12), 5944-5948, DOI: 10.1021/nl403036h.

(12) Song, Z.; Schultz, T.; Ding, Z.; Lei, B.; Han, C.; Amsalem, P.; Lin, T.; Chi, D.; Wong, S. L.; Zheng, Y. J.; et al. Electronic Properties of a 1D Intrinsic/p-Doped Heterojunction in a 2D Transition Metal Dichalcogenide Semiconductor. *ACS Nano* **2017**, *11* (9), 9128-9135, DOI: 10.1021/acsnano.7b03953.

(13) Ji, H. G.; Solis-Fernandez, P.; Yoshimura, D.; Maruyama, M.; Endo, T.; Miyata, Y.; Okada, S.; Ago, H. Chemically Tuned p- and n-Type WSe(2) Monolayers with High Carrier Mobility for Advanced Electronics. *Adv Mater* **2019**, *31* (42), e1903613, DOI: 10.1002/adma.201903613.

(14) Kiriya, D.; Tosun, M.; Zhao, P.; Kang, J. S.; Javey, A. Air-stable surface charge transfer doping of MoS(2) by benzyl viologen. *J Am Chem Soc* **2014**, *136* (22), 7853-7856, DOI: 10.1021/ja5033327.

(15) Chamlagain, B.; Withanage, S. S.; Johnston, A. C.; Khondaker, S. I. Scalable lateral heterojunction by chemical doping of 2D TMD thin films. *Sci Rep* **2020**, *10* (1), 12970, DOI: 10.1038/s41598-020-70127-6.

(16) Lin, J. D.; Han, C.; Wang, F.; Wang, R.; Xiang, D.; Qin, S.; Zhang, X. A.; Wang, L.; Zhang, H.; Wee, A. T.; et al. Electron-doping-enhanced trion formation in monolayer molybdenum disulfide functionalized with cesium carbonate. *ACS Nano* **2014**, *8* (5), 5323-5329, DOI: 10.1021/nn501580c.

(17) Yang, L.; Majumdar, K.; Liu, H.; Du, Y.; Wu, H.; Hatzistergos, M.; Hung, P. Y.; Tieckelmann, R.; Tsai, W.; Hobbs, C.; et al. Chloride molecular doping technique on 2D materials: WS2 and MoS2. *Nano Lett* **2014**, *14* (11), 6275-6280, DOI: 10.1021/nl502603d.

(18) Fang, H.; Tosun, M.; Seol, G.; Chang, T. C.; Takei, K.; Guo, J.; Javey, A. Degenerate n-doping of few-layer transition metal dichalcogenides by potassium. *Nano Lett* **2013**, *13* (5), 1991-1995, DOI: 10.1021/nl400044m.

(19) Jeong, I.; Cho, K.; Yun, S.; Shin, J.; Kim, J.; Kim, G. T.; Lee, T.; Chung, S. Tailoring the Electrical Characteristics of MoS(2) FETs through Controllable Surface Charge Transfer Doping Using Selective Inkjet Printing. *ACS Nano* **2022**, *16* (4), 6215-6223, DOI: 10.1021/acsnano.2c00021.

(20) Brinkmann, H.; Kelting, C.; Makarov, S.; Tsaryova, O.; Schnurpfeil, G.; Wöhrle, D.; Schlettwein, D. Fluorinated phthalocyanines as molecular semiconductor thin films. *Phys. Status Solidi A* **2008**, *205* (3), 409-420, DOI: 10.1002/pssa.200723391.

(21) Lindner, S.; Treske, U.; Grobosch, M.; Knupfer, M. Charge transfer at F16CoPc and CoPc interfaces to Au. *Appl. Phys. A* **2011**, *105* (4), 921-925, DOI: 10.1007/s00339-011-6648-x.

(22) Greulich, K.; Belser, A.; Bölke, S.; Grüninger, P.; Karstens, R.; Sättele, M. S.; Ovsyannikov, R.; Giangrisostomi, E.; Basova, T. V.; Klyamer, D.; et al. Charge Transfer from Organic Molecules to Molybdenum Disulfide: Influence of the Fluorination of Iron Phthalocyanine. *J. Phys. Chem. C* **2020**, *124* (31), 16990-16999, DOI: 10.1021/acs.jpcc.0c03862.

(23) Pak, J.; Jang, J.; Cho, K.; Kim, T. Y.; Kim, J. K.; Song, Y.; Hong, W. K.; Min, M.; Lee, H.; Lee, T. Enhancement of photodetection characteristics of MoS2 field effect transistors using surface treatment with copper phthalocyanine. *Nanoscale* **2015**, *7* (44), 18780-18788, DOI: 10.1039/c5nr04836b.

(24) Pak, J.; Min, M.; Cho, K.; Lien, D.-H.; Ahn, G. H.; Jang, J.; Yoo, D.; Chung, S.; Javey, A.; Lee, T. Improved photoswitching response times of MoS2 field-effect transistors by stacking p-type copper phthalocyanine layer. *Appl. Phys. Lett.* **2016**, *109* (18), 183502, DOI: 10.1063/1.4966668.

(25) Andleeb, S.; Wang, X.; Dong, H.; Valligatla, S.; Saggau, C. N.; Ma, L.; Schmidt, O. G.; Zhu, F. Fast-Response Micro-Phototransistor Based on MoS2/Organic Molecule Heterojunction. In *Nanomaterials*, **2023**, *13* (9), 1491.

(26) Huang, Y.; Zhuge, F.; Hou, J.; Lv, L.; Luo, P.; Zhou, N.; Gan, L.; Zhai, T. Van der Waals Coupled Organic Molecules with Monolayer MoS(2) for Fast Response Photodetectors with Gate-Tunable Responsivity. *ACS Nano* **2018**, *12* (4), 4062-4073, DOI: 10.1021/acsnano.8b02380.

(27) Mutz, N.; Park, S.; Schultz, T.; Sadofev, S.; Dalgleish, S.; Reissig, L.; Koch, N.; List-Kratochvil, E. J. W.; Blumstengel, S. Excited-State Charge Transfer Enabling MoS2/Phthalocyanine Photodetectors with Extended Spectral Sensitivity. *J. Phys. Chem. C* **2020**, *124* (5), 2837-2843, DOI: 10.1021/acs.jpcc.9b10877.

(28) Park, J. H.; Sanne, A.; Guo, Y.; Amani, M.; Zhang, K.; Movva, H. C. P.; Robinson, J. A.; Javey, A.; Robertson, J.; Banerjee, S. K.; et al. Defect passivation of transition metal dichalcogenides via a charge transfer van der Waals interface. *Sci Adv* **2017**, *3* (10), e1701661, DOI: 10.1126/sciadv.1701661.

(29) Amsterdam, S. H.; Stanev, T. K.; Wang, L.; Zhou, Q.; Irgen-Gioro, S.; Padgaonkar, S.; Murthy, A. A.; Sangwan, V. K.; Dravid, V. P.; Weiss, E. A.; et al. Mechanistic Investigation of Molybdenum Disulfide Defect Photoluminescence Quenching by Adsorbed Metallophthalocyanines. *J Am Chem Soc* **2021**, *143* (41), 17153-17161, DOI: 10.1021/jacs.1c07795.

(30) Padgaonkar, S.; Amsterdam, S. H.; Bergeron, H.; Su, K.; Marks, T. J.; Hersam, M. C.; Weiss, E. A. Molecular-Orientation-Dependent Interfacial Charge Transfer in Phthalocyanine/MoS2 Mixed-Dimensional Heterojunctions. *J. Phys. Chem. C* **2019**, *123* (21), 13337-13343, DOI: 10.1021/acs.jpcc.9b04063.

(31) Benjamin, C. J.; Zhang, S.; Chen, Z. Controlled doping of transition metal dichalcogenides by metal work function tuning in phthalocyanine compounds. *Nanoscale* **2018**, *10* (11), 5148-5153, DOI: 10.1039/c7nr08497h.

(32) Kong, Y.; Obaidulla, S. M.; Habib, M. R.; Wang, Z.; Wang, R.; Khan, Y.; Zhu, H.; Xu, M.; Yang, D. Interlayer exciton emission in a MoS(2)/VOPc inorganic/organic van der Waals heterostructure. *Mater Horiz* **2022**, *9* (4), 1253-1263, DOI: 10.1039/d1mh01622a.

(33) Banerjee, A.; Kundu, B.; Pal, A. J. Hybrid heterojunctions between a 2D transition metal dichalcogenide and metal phthalocyanines: their energy levels vis-a-vis current rectification. *Phys Chem Chem Phys* **2017**, *19* (41), 28450-28457, DOI: 10.1039/c7cp05470j.

(34) Kafle, T. R.; Kattel, B.; Yao, P.; Zereshki, P.; Zhao, H.; Chan, W. L. Effect of the Interfacial Energy Landscape on Photoinduced Charge Generation at the ZnPc/MoS(2) Interface. *J Am Chem Soc* **2019**, *141* (28), 11328-11336, DOI: 10.1021/jacs.9b05893.

(35) Liu, X. Y.; Xie, X. Y.; Fang, W. H.; Cui, G. Theoretical Insights into Interfacial Electron Transfer between Zinc Phthalocyanine and Molybdenum Disulfide. *J Phys Chem A* **2018**, *122* (50), 9587-9596, DOI: 10.1021/acs.jpca.8b07816.

(36) Giangrisostomi, E.; Ovsyannikov, R.; Sorgenfrei, F.; Zhang, T.; Lindblad, A.; Sassa, Y.; Cappel, U. B.; Leitner, T.; Mitzner, R.; Svensson, S.; et al. Low Dose Photoelectron Spectroscopy at BESSY II: Electronic structure of matter in its native state. *J Electron Spectros Relat Phenomena* **2018**, *224*, 68-78, DOI: 10.1016/j.elspec.2017.05.011.

(37) Vollmer, A.; Ovsyannikov, R.; Gorgoi, M.; Krause, S.; Oehzelt, M.; Lindblad, A.; Mårtensson, N.; Svensson, S.; Karlsson, P.; Lundvuist, M.; et al. Two dimensional band structure mapping of organic single crystals using the new generation electron energy analyzer ARTOF. *J Electron Spectros Relat Phenomena* **2012**, *185* (3-4), 55-60, DOI: 10.1016/j.elspec.2012.01.003.

(38) Lucovsky, G.; White, R. M.; Benda, J. A.; Revelli, J. F. Infrared-Reflectance Spectra of Layered Group-IV and Group-VI Transition-Metal Dichalcogenides. *Physical Review B* **1973**, *7* (8), 3859-3870, DOI: 10.1103/PhysRevB.7.3859.

(39) Yeh, J. J.; Lindau, I. Atomic subshell photoionization cross sections and asymmetry parameters: 1 ⩽ Z ⩽ 103. *At. Data Nucl. Data Tables* **1985**, *32* (1), 1-155, DOI: 10.1016/0092-640x(85)90016-6.

(40) Seah, M. P.; Dench, W. A. Quantitative electron spectroscopy of surfaces: A standard data base for electron inelastic mean free paths in solids. *Surf Interface Anal* **2004**, *1* (1), 2-11, DOI: 10.1002/sia.740010103.

(41) Aygül, U.; Hintz, H.; Egelhaaf, H.-J.; Distler, A.; Abb, S.; Peisert, H.; Chassé, T. Energy Level Alignment of a P3HT/Fullerene Blend during the Initial Steps of Degradation. *J. Phys. Chem. C* **2013**, *117* (10), 4992-4998, DOI: 10.1021/jp4004642.

(42) Late, D. J.; Liu, B.; Matte, H. S.; Dravid, V. P.; Rao, C. N. Hysteresis in single-layer MoS2 field effect transistors. *ACS Nano* **2012**, *6* (6), 5635-5641, DOI: 10.1021/nn301572c.

(43) Gould, R. D. Structure and electrical conduction properties of phthalocyanine thin films. *Coord. Chem. Rev.* **1996**, *156*, 237-274, DOI: 10.1016/s0010-8545(96)01238-6.

(44) Niebur, A.; Soll, A.; Haizmann, P.; Strolka, O.; Rudolph, D.; Tran, K.; Renz, F.; Frauendorf, A. P.; Hubner, J.; Peisert, H.; et al. Untangling the intertwined: metallic to semiconducting phase transition of colloidal MoS(2) nanoplatelets and nanosheets. *Nanoscale* **2023**, *15* (12), 5679-5688, DOI: 10.1039/d3nr00096f.

(45) Eda, G.; Yamaguchi, H.; Voiry, D.; Fujita, T.; Chen, M.; Chhowalla, M. Photoluminescence from chemically exfoliated MoS2. *Nano Lett* **2011**, *11* (12), 5111-5116, DOI: 10.1021/nl201874w.

(46) Lu, C. P.; Li, G.; Mao, J.; Wang, L. M.; Andrei, E. Y. Bandgap, mid-gap states, and gating effects in MoS2. *Nano Lett* **2014**, *14* (8), 4628-4633, DOI: 10.1021/nl501659n.

(47) Giangrisostomi, E.; Ovsyannikov, R.; Haverkamp, R.; Sorgenfrei, N. L. A. N.; Neppl, S.; Sezen, H.; Johansson, F. O. L.; Svensson, S.; Föhlisch, A. Inhomogeneity of Cleaved Bulk MoS2 and Compensation of Its Charge Imbalances by Room-Temperature Hydrogen Treatment. *Adv. Mater. Interfaces* **2023**, *10* (32), 2300392, DOI: 10.1002/admi.202300392.

(48) He, T.; Ding, H.; Peor, N.; Lu, M.; Corley, D. A.; Chen, B.; Ofir, Y.; Gao, Y.; Yitzchaik, S.; Tour, J. M. Silicon/molecule interfacial electronic modifications. *J Am Chem Soc* **2008**, *130* (5), 1699-1710, DOI: 10.1021/ja0768789.

(49) Rückerl, F.; Klaproth, T.; Schuster, R.; Büchner, B.; Knupfer, M. Surface functionalization of WSe2 by F16CoPc. *Phys. Status Solidi B* **2016**, *254* (6), 1600656, DOI: 10.1002/pssb.201600656.

(50) Kam, K. K.; Parkinson, B. A. Detailed photocurrent spectroscopy of the semiconducting group VIB transition metal dichalcogenides. *J. Phys. Chem.* **2002**, *86* (4), 463-467, DOI: 10.1021/j100393a010.

23

(51) Ueno, N.; Kera, S. Electron spectroscopy of functional organic thin films: Deep insights into valence electronic structure in relation to charge transport property. *Prog. Surf. Sci.* **2008**, *83* (10-12), 490-557, DOI: 10.1016/j.progsurf.2008.10.002.

(52) Shang, M.-H.; Nagaosa, M.; Nagamatsu, S.-i.; Hosoumi, S.; Kera, S.; Fujikawa, T.; Ueno, N. Photoemission from valence bands of transition metal-phthalocyanines. *J Electron Spectros Relat Phenomena* **2011**, *184* (3-6), 261-264, DOI: 10.1016/j.elspec.2010.10.006.

(53) Schönauer, K.; Weiss, S.; Feyer, V.; Lüftner, D.; Stadtmüller, B.; Schwarz, D.; Sueyoshi, T.; Kumpf, C.; Puschnig, P.; Ramsey, M. G.; et al. Charge transfer and symmetry reduction at the CuPc/Ag(110) interface studied by photoemission tomography. *Physical Review B* **2016**, *94* (20), 205144, DOI: 10.1103/PhysRevB.94.205144.

(54) Peisert, H.; Kolacyak, D.; Chassé, T. Site-Specific Charge-Transfer Screening at Organic/Metal Interfaces. *J. Phys. Chem. C* **2009**, *113* (44), 19244-19250, DOI: 10.1021/jp9057548.

(55) Chiang, T.; Kaindl, G.; Mandel, T. Layer-resolved shifts of photoemission and Auger spectra from physisorbed rare-gas multilayers. *Phys Rev B Condens Matter* **1986**, *33* (2), 695-711, DOI: 10.1103/physrevb.33.695.

(56) Ueno, N.; Kera, S.; Sakamoto, K.; Okudaira, K. K. Energy band and electron-vibration coupling in organic thin films: photoelectron spectroscopy as a powerful tool for studying the charge transport. *Appl. Phys. A* **2008**, *92* (3), 495-504, DOI: 10.1007/s00339-008-4553-8.

(57) Peisert, H.; Knupfer, M.; Schwieger, T.; Auerhammer, J. M.; Golden, M. S.; Fink, J. Full characterization of the interface between the organic semiconductor copper phthalocyanine and gold. *J. Appl. Phys.* **2002**, *91* (8), 4872-4878, DOI: 10.1063/1.1459620.

(58) Braun, S.; Salaneck, W. R. Fermi level pinning at interfaces with tetrafluorotetracyanoquinodimethane (F4-TCNQ): The role of integer charge transfer states. *Chem. Phys. Lett.* **2007**, *438* (4-6), 259-262, DOI: 10.1016/j.cplett.2007.03.005.

(59) Braun, S.; Salaneck, W. R.; Fahlman, M. Energy-Level Alignment at Organic/Metal and Organic/Organic Interfaces. *Adv. Mater.* **2009**, *21* (14-15), 1450-1472, DOI: 10.1002/adma.200802893.

(60) Braun, S.; Liu, X.; Salaneck, W. R.; Fahlman, M. Fermi level equilibrium at donor–acceptor interfaces in multi-layered thin film stack of TTF and TCNQ. *Org. Electron.* **2010**, *11* (2), 212-217, DOI: 10.1016/j.orgel.2009.10.018.

(61) Gruenewald, M.; Schirra, L. K.; Winget, P.; Kozlik, M.; Ndione, P. F.; Sigdel, A. K.; Berry, J. J.; Forker, R.; Brédas, J.-L.; Fritz, T.; et al. Integer Charge Transfer and Hybridization at an Organic Semiconductor/Conductive Oxide Interface. *J. Phys. Chem. C* **2015**, *119* (9), 4865-4873, DOI: 10.1021/jp512153b.

(62) Hofmann, O. T.; Rinke, P.; Scheffler, M.; Heimel, G. Integer versus Fractional Charge Transfer at Metal(/Insulator)/Organic Interfaces: Cu(/NaCl)/TCNE. *ACS Nano* **2015**, *9* (5), 5391-5404, DOI: 10.1021/acsnano.5b01164.

(63) Hofmann, O. T.; Deinert, J. C.; Xu, Y.; Rinke, P.; Stahler, J.; Wolf, M.; Scheffler, M. Large work function reduction by adsorption of a molecule with a negative electron affinity: pyridine on ZnO(1010). *J Chem Phys* **2013**, *139* (17), 174701, DOI: 10.1063/1.4827017.

(64) Erker, S.; Hofmann, O. T. Fractional and Integer Charge Transfer at Semiconductor/Organic Interfaces: The Role of Hybridization and Metallicity. *J Phys Chem Lett* **2019**, *10* (4), 848-854, DOI: 10.1021/acs.jpclett.8b03857.

(65) Vázquez, H.; Oszwaldowski, R.; Pou, P.; Ortega, J.; Pérez, R.; Flores, F.; Kahn, A. Dipole formation at metal/PTCDA interfaces: Role of the Charge Neutrality Level. *EPL* **2004**, *65* (6), 802-808, DOI: 10.1209/epl/i2003-10131-2.

(66) Vázquez, H.; Flores, F.; Oszwaldowski, R.; Ortega, J.; Pérez, R.; Kahn, A. Barrier formation at metal–organic interfaces: dipole formation and the charge neutrality level. *Appl. Surf. Sci.* **2004**, *234* (1-4), 107-112, DOI: 10.1016/j.apsusc.2004.05.084.

(67) Wager, J. F.; Kuhn, K. Device Physics Modeling of Surfaces and Interfaces from an Induced Gap State Perspective. *Crit. Rev. Solid State Mater. Sci.* **2016**, *42* (5), 373-415, DOI: 10.1080/10408436.2016.1223013.

24

(68) Chen, W.; Qi, D.; Gao, X.; Wee, A. T. S. Surface transfer doping of semiconductors. *Prog. Surf. Sci.* **2009**, *84* (9-10), 279-321, DOI: 10.1016/j.progsurf.2009.06.002.

(69) Ules, T.; Lüftner, D.; Reinisch, E. M.; Koller, G.; Puschnig, P.; Ramsey, M. G. Orbital tomography of hybridized and dispersing molecular overlayers. *Phys. Rev. B* **2014**, *90* (15), 155430, DOI: 10.1103/PhysRevB.90.155430.

(70) Peisert, H.; Uihlein, J.; Petraki, F.; Chassé, T. Charge transfer between transition metal phthalocyanines and metal substrates: The role of the transition metal. *J Electron Spectros Relat Phenomena* **2015**, *204*, 49-60, DOI: 10.1016/j.elspec.2015.01.005.

(71) Uihlein, J.; Polek, M.; Glaser, M.; Adler, H.; Ovsyannikov, R.; Bauer, M.; Ivanovic, M.; Preobrajenski, A. B.; Generalov, A. V.; Chassé, T.; et al. Influence of Graphene on Charge Transfer between CoPc and Metals: The Role of Graphene–Substrate Coupling. *J. Phys. Chem. C* **2015**, *119* (27), 15240-15247, DOI: 10.1021/acs.jpcc.5b02912.

(72) Belser, A.; Greulich, K.; Grüninger, P.; Karstens, R.; Ovsyannikov, R.; Giangrisostomi, E.; Nagel, P.; Merz, M.; Schuppler, S.; Chassé, T.; et al. Perfluorinated Phthalocyanines on Cu(110) and Cu(110)-(2 × 1)O: The Special Role of the Central Cobalt Atom. *J. Phys. Chem. C* **2021**, *125* (16), 8803-8814, DOI: 10.1021/acs.jpcc.1c01215.

(73) Schmid, M.; Kaftan, A.; Steinrück, H.-P.; Gottfried, J. M. The electronic structure of cobalt(II) phthalocyanine adsorbed on Ag(111). *Surf. Sci.* **2012**, *606* (11-12), 945-949, DOI: 10.1016/j.susc.2012.02.012.

(74) Vlček, J.; Kühne, I. A.; Zákutná, D.; Marešová, E.; Fekete, L.; Otta, J.; Fitl, P.; Vrňata, M. Temperature-dependent phase composition of fluorinated zinc phthalocyanine thin films and their sensing properties towards gaseous NO2. *CrystEngComm* **2021**, *23* (41), 7237-7244, DOI: 10.1039/d1ce01014j.

(75) Brendel, M.; Krause, S.; Steindamm, A.; Topczak, A. K.; Sundarraj, S.; Erk, P.; Höhla, S.; Fruehauf, N.; Koch, N.; Pflaum, J. The Effect of Gradual Fluorination on the Properties of FnZnPc Thin Films and FnZnPc/C60 Bilayer Photovoltaic Cells. *Adv. Funct. Mater.* **2015**, *25* (10), 1565-1573, DOI: 10.1002/adfm.201404434.

(76) Chen, W.; Kahn, A.; Mangat, P. S.; Soukiassian, P.; Florez, L. T.; Harbison, J. P.; Palmstrom, C. J. Pb/GaAs(100): Band bending, adatom-induced gap states and surface dipole. *J. Vac. Sci. Technol. B* **1993**, *11* (4), 1571-1574, DOI: 10.1116/1.586971.

(77) Shen, C.; Kahn, A. The role of interface states in controlling the electronic structure of Alq3/reactive metal contacts. *Org. Electron.* **2001**, *2* (2), 89-95, DOI: 10.1016/s1566-1199(01)00015-5.

(78) Shinotsuka, H.; Tanuma, S.; Powell, C. J.; Penn, D. R. Calculations of electron inelastic mean free paths. XII. Data for 42 inorganic compounds over the 50 eV to 200 keV range with the full Penn algorithm. *Surf Interface Anal* **2018**, *51* (4), 427-457, DOI: 10.1002/sia.6598.

(79) Seah, M. P. An accurate and simple universal curve for the energy-dependent electron inelastic mean free path. *Surf Interface Anal* **2011**, *44* (4), 497-503, DOI: 10.1002/sia.4816.